RSC Advances

ROYAL SOCIETY OF CHEMISTRY

www.rsc.org/advances

Journal Name

RSCPublishing

ARTICLE

www.rsc.org/

N-phenylaminomethyl hybrid silica, a better alternative to achieve reinforced PU nanocomposites

Qiuhong Zhang, [abc] Xin Huang, [abc] Zhen Meng, [a] Xudong Jia* [abc] and Kai Xi*[b]

A novel N-phenylaminomethyl silica (NPAM-silica) was firstly synthesized by one-step emulsion polymerization of N-phenylaminomethyltriethoxysilane (ND-42). The hybrid silica could be dispersed in a variety of organic solvents including THF, acetone, DMF and DMAC. The NPAM-silica was mainly composed of fully condensed silsesquioxanes and a small quantity of partially condensed silsesquioxanes which was confirmed by ^{29}SiNMR and MALDI-TOF MS. GPC showed that the polydispersity of the NPAM-silica was 1.08. It was then introduced into polyurethane (PU) as a chemical cross-linker. The high reactivity of NPAM-silica was investigated by means of solid state Nuclear Magnetic Resonance (SSNMR). TEM and AFM showed that the NPAM-silica was nano-dispersed in the hard segments region of PU. Mechanical property of NPAM-silica/PU nanocomposites at rubber state was enhanced when NPAM-silica was added, which was reflected in DMA and tensile tests at constant T_{test}-T_g. It is also concluded that the increase of the modulus was derived from both the nanofiller contribution and entropic contribution which were test by temperature dependence of modulus at rubber region. NPAM-silica/PU possessed higher storage modulus at the rubber plateau than that of N-phenylaminomethyl POSS/PU when the loading was below 26wt%. The homogeneity of NPAM-silica/PU was better than that of N-phenylaminomethyl POSS/PU which was characterized by TEM and small angle x-ray scattering (SAXS). The NPAM-silica showed greater advantage in practical application compared with N-phenylaminomethyl POSS.

Introduction

Polymer nanocomposites have been intensively studied in the past decades because the nanofillers offer the promise of polymer composites with promoted properties.[1, 2] The key points to promotion are the way nanofiller integrated into a polymer and dispersion degree of nanofiller. The favorable effects are evident when nanofillers are integrated into a polymer via a chemical reaction because chemical bonding can enhance the compatibility between fillers and polymer matrix. An adequate amount and type of filler such as clay[3], carbon black[4, 5] and silica[6-8] were chosen to add into polymer matrix to tune the properties. However, due to the incompatibility between filler and polymer, phase separation may be induced and the amount of the additives was limited[9], hindering applications of composites in coatings. Lots of work had been done to improve the compatibility of polymers and nanofillers.[10-14] Organic silanes are often used as precursors to chemically modify inorganic fillers. However, overdue silane of modifying inorganic fillers often necessitates extensive cleaning, and the particle surfaces can be only partially modified which results in inhomogeneity of the functional fillers. Besides, aggregates would happen in polymer matrix during the solvent evaporated process. These will result in the poor dispersion degree of filler in polymer matrix. Therefore, it is meaningful to find novel economic additives that can not only improve compatibility between fillers and polymer but also enhance properties of composite.

Silsesquioxanes are an important class of organic-inorganic hybrids containing the organic functional groups inherently and uniformly. Recently, considerable literature has grown up relating to the polyhedral oligomeric silsesquioxanes (POSS), with which the mechanical and thermal properties can be enhanced. [15-18] But, because of its cost, it is limited in practical use. A much easier and economic route to synthesize silsesquioxanes with the appropriate properties is still needed. Though POSS may enhance the mechanical and thermal properties of POSS/polymer nanocomposites, it is hard for POSS to disperse in polymer in molecular level due to the immiscibility and crystallization of POSS.[19] In physical blending system such as PLA/POSS, the diameters of POSS were ranging from 100 nm to 200 nm.[20] In random POSS copolymers, the POSS moieties had been found to aggregate into nano-crystalline domains of 10-100 nm.[21] For

multifunctional POSS/polymer composites, when the amount of POSS was above a certain value, it would also aggregate[22] or even form nanocrystals[23, 24] due to POSS-POSS interactions. The crystallization will sacrifice the dispersibility and the inner functional groups of POSS will not take part in the reaction.

One of the possible ways to overcome the problems may be the application of a mixture of reactive silsesquioxanes instead of mono-dispersed POSS. Mori and coworkers[25, 26] had reported a series of silsesquioxane based silica nanoparticles with a very high yield, which was derived from hydrolytic condensation of organic silane. Bliznyuk[27] used the same method to synthesize the silsesquioxane based nanoparticles and found the nanoparticles were 2-4 nm dispersed in polyurethane matrix providing a new idea to prepare similar POSS mixtures. Silsesquioxanes were also prepared by environmental friendly methods.[28, 29] Lee[30] used a simple emulsion process to prepare an attractive hybrid silica with high yield. It could be used in polymer/nanocomposites with lower costs. Though hybrid silica has been used in several fields such as ceramics, magnets,[31] semiconductors,[32] and chromatographic adsorbents,[33] hybrid silica applied in polymer/nanocomposites is still less-reported.[34]

PU is one of the most commercial elastomers that can be used as adhesives, flexible films, coatings, or hard plastics.[35] Despite its high wear resistance and good toughness, the low modulus and poor heat resistance of PU limit its scope of application.[9] The effective methods to improve the mechanical and thermal properties of PU are to introduce fillers into PU matrix [36] and increase crosslinking densities of PU.[37]

In our previous work, we reported a simple route to synthesize N-phenylaminomethyl POSS, which was then used as a cross-linker to incorporate to conventional PU.[38] In this work, we report the synthesis of new *N*-phenylaminomethyl hybrid silica with a facile route and its structure was confirmed by NMR, MALDITOF-MS and GPC. The as-prepared hybrid silica was then introduced into polyurethane. The morphology of NPAM-silica/PU nanocomposites was investigated by TEM and AFM. Thermo-mechanical properties of the nanocomposites were investigated by DMA and tensile tests. Besides, the thermal-mechanical properties and morphologies of NPAM-silica/PU were compared with those of N-phenylaminomethyl POSS/PU. The purpose of this paper is to provide a new alternative for polymer/nanocomposite in practical application.

Experiment section

Materials

N-Phenylaminomethyltriethoxysilane (ND-42) and Phenyltriethoxysilane were acquired from Liyang Mingtian Chemical Corporation, China. Ammonium hydroxide and sodium dodecylbenzene sulfonate (SDBS) were supplied by Jiangsu Yonghua Fine Chemistry Co. Ltd., China. All chemicals were used as received without further purification. Water was obtained from a Sartorius arium 611DI water purification system. Stannous octoate was obtained from Shanghai Guoyao Corporation, China. Polytetramethylene glycol (PTMG, M_n=1000), isophorone diisocyanate (IPDI) and 1,4-butanediol (BD) were supplied by Sigma-Aldrich (USA) and dried under vacuum before use. *N,N*-dimethylacetamide (DMAC, Shanghai Guoyao Corporation, China) was dried by BaO and vacuum transferred.

Synthesis of NPAM-silica and Phenyl-silica

The synthetic route of NPAM-silica was shown in Scheme 1. 5.40 g of ND-42 and 0.013 g of SDBS were added into 30 ml of water under vigorous stirring until an emulsion formed. 0.5 ml of $NH_3{\cdot}H_2O$ was dropwise added to the emulsion (pH=11.5), and the reaction was kept at 50 °C for 48 h. A homogeneous emulsion was obtained. The concentration of SDBS used in the preparation of the sample was 0.2 critical micelle concentrations (CMC).

The synthetic route of Phenyl-silica was the same as that of NPAM-silica. 5.40 g of Phenyltriethoxysilane and 0.013 g of SDBS were added into 30 ml of water under vigorous stirring until an emulsion formed. 0.5 ml of $NH_3{\cdot}H_2O$ was dropwise added to the emulsion (pH=11.5), and the reaction was kept at 50 °C for 48 h. A homogeneous emulsion was obtained.

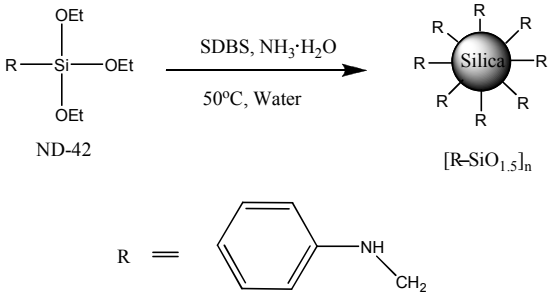

Scheme 1. Synthetic route for NPAM-silica by hydrolytic condensation of ND-42.

Synthesis of NPAM-silica/PU Nanocomposites

The nanocomposites were synthesized according to the literature.[18] The details are described below: The reference prepolymer was synthesized by dissolving polytetramethylene ether glycol (PTMG) (3.00 g, 0.003 mol) and isophorone diisocyanate (IPDI) (1.33 g, 0.006 mol) in a 100 ml three-necked flask equipped with mechanical stirrer under nitrogen atmosphere. Stannous octoate (0.1 wt %) was added as catalyst and the reaction was kept stirring at 85°C for 4 h to obtain the prepolymer which was viscous liquid. The prepolymer was then dissolved in 10 ml of DMAC. Various amounts of NPAM-silica were dissolved in DMAC (10 ml), and the solutions were added into the prepolymer solution and kept stirring for 10 minutes at 95°C. BD dissolved in 10 ml of DMAC was then added to the mixture. The amount of BD was accordingly adjusted in order to keep the NCO / (OH + NH) = 1 for PU11. The amount of NH of PU18 was equivalent with NCO, so BD was not added. BD was not added for PU26 and PU40 either, because NH / NCO exceeded 1. With stirring for 5 min, the mixture was poured into a PTFE plate. After the majority of the solvent was evaporated under vacuum at 60°C, the plates were put in an oven and kept at 95°C for 12 h to complete the reaction. At last the NPAM-silica/PU films were obtained (Scheme 2). PU 11 +

7 (UnR) was synthesized to compare temperature dependence modulus with PU 11 and PU 18. 11 wt% NPAM-silica and 7 wt% Phenyl-silica were added to the PU prepolymer and kept stirring for 10 minutes at 95°C. BD dissolved in 10 ml of DMAC was then added to the mixture. The amount of BD was also accordingly adjusted in order to keep the NCO / (OH + NH) = 1. With stirring for 5 min, the mixture was poured into a PTFE plate. The post-process method was the same as that of PU 11. The compositions of neat PU and NPAM-silica/PU nanocomposites were listed in Table 1.

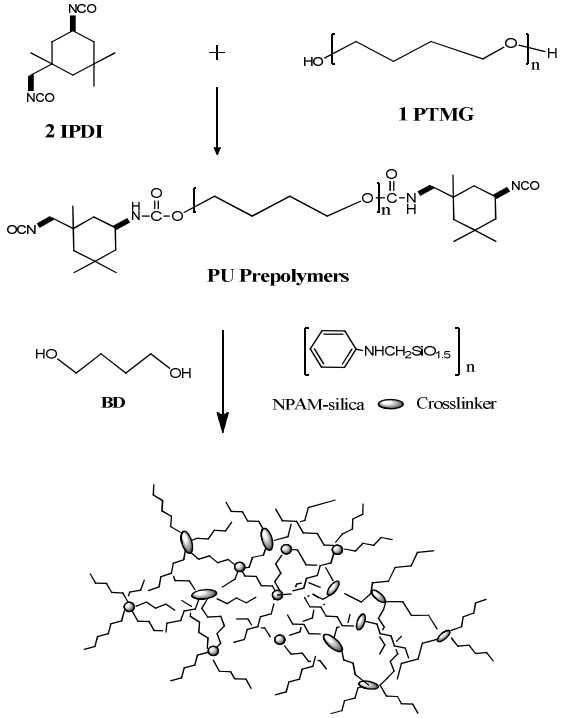

Scheme 2. Synthesis of NPAM-silica/PU nanocomposites.

Table 1. Compositions of Neat PU and NPAM-silica/PU Composites.

Sample	NPAM-Silica	Ph-silica	IPDI	PTMG	BD
	wt%	wt%	wt%	wt%	wt%
Neat PU	0	0	28.9	65.2	5.9
PU11	11.4	0	26.6	60.0	2.2
PU11+7(UnR)	11.4	7	26.6	60.0	2.2
PU18	18.0	0	25.2	56.8	0
PU26	26.0	0	22.8	51.2	0
PU40	40.0	0	18.5	41.5	0

Characterization

Solid state ^{13}C-NMR and ^{29}Si-NMR spectra were recorded on a Bruker Avance 400 NMR spectrometer at 399.7 MHz using a 7 mm T3 double resonance CPMAS probe and a zirconia PENCIL rotor. All of the experiments were carried out at room temperature. Solution ^{13}C-NMR and ^{29}Si-NMR spectra were recorded on a Bruker DRX NMR spectrometer at 500 MHz, and tetramethylsilane (TMS) was used as internal standard.

Wide-angle X-ray diffraction experiments (XRD) of NPAM-silica was carried out on a Bruke D8 Advance with Cu KR radiation (1.541Å), scanning from (2θ) 2° to 50° with step size 0.02 and time per step 4s.

Gel permeation chromatography (GPC) was performed at room temperature on a Waters 515 equipped with a Wyatt Technology Optilab Rex refractive index detector. The columns were STYRAGEL HR3, HR4 and HR5 (300×7.8 mm) from Waters. Tetrahydrofuran (THF, HPLC grade, Aldrich) was used as solvent at a flow rate of 1 ml/min. Sample solutions in THF were filtered over a filter with pore size of 0.45 μm (Nylon, Millex-HN 13 mm Syringes Filters, Millipore, USA). The columns were calibrated by using polystyrene standards with molecular weights in the range of 900 and 1.74×10^6 g/mol (with NMD for 1.02-1.11).

Matrix Assisted Laser Desorption Ionization Time of Flight Mass Spectrometry (MALDI-TOF MS) was performed using a Bruker Daltonics Autoflex TOF/TOF in linear and reflectron modes. The matrix 2, 5-dihydroxybenzoic acid (DHBA) was dissolved in THF (10 mg/ml), and mixed with the sample solution (1 mg/ml in THF) in 1:1 v/v ratio. Samples were spotted onto the target and dried in air.

The Fourier transform infrared spectra (FTIR) were recorded on a NICOLET NEXUS 870 spectrophotometer. The attenuated total reflection (ATR) accessories were used to measure the FTIR spectra of all the specimens on fresh surfaces. In all cases, 64 scans at a resolution of 2 cm^{-1} were used to record spectra.

The morphology of silica/PU composites was measured by HRTEM. The materials were frozen to -100 °C, and ultrathin sections were made by using a Leica ULTRACUT UC6 with approximate thickness about 70 nm. The sections were collected onto copper grids. The grids were then imaged using a JEM-2100 transmission electron microscope at 200 kV. Surface topographies were also characterized by atomic force microscopy (AFM) in tapping mode using silicon tips with Olympus OMCL-AC160TS and controller from Veeco Corporation. Samples were dropped onto the silicon wafer surfaces by DMAC solutions of polymer films (1 wt%) and cured in a vacuum oven at 95 °C for 12 h.

The tensile tests were carried out on an Instron Series IX Automated Materials Testing System (Instron 4466, UK). The mechanical properties were measured according to ASTM D1708 standard method. Young's Modulus was obtained by calculating the slop of the initial part (< 5% strain). Tests were performed in triplicate to give mean values. The dynamic mechanical tests were carried out on a Dynamic Mechanical Analyzer (DMA) (METRAVIB DMA+450， France). The viscoelastic properties were measured under a nitrogen atmosphere, at a heating rate of 2 K /min from -120 °C to 200 °C and a frequency of 10 Hz. The experiments were carried out until the samples became too soft to be tested.

SAXS was performed on an Anton Paar SAXSess at room temperature. The experiment was carried out by simultaneously recording the data on an imaging-plate (IP) which extended to high-angle range (the q range covered by the IP was from 0.1 to 29 nm^{-1}, $q=4\pi\sin\theta/\lambda$, where the wavelength λ was 0.1542 nm of

Cu-Kα radiation and 2θ was the scattering angle) at 40 kV and 40 mA for 5 min.

Results and Discussions

1. The synthesis of novel NPAM-silica

The synthetic route was facile and the emulsion was stabilized by ammonia. The NPAM-silica was monodispersed nanosphere characterized by TEM and SEM (Figure 1). DLS result also confirmed the monodispersity of NPAM-silica (Fig. S1, ESI). The size of the nanosphere could be controlled between 40 nm to 200 nm by adding different amounts of surfactants with 1.0 CMC to 0.2 CMC. Here, we chose 0.2 CMC of the surfactant typically and the size of nanosphere was about 200 nm.

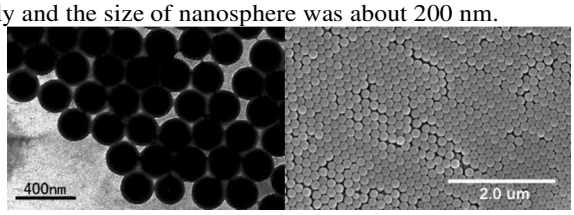

Figure 1. TEM (left, scale bar 400 nm) and SEM (right, scale bar 2.0 μm) pictures of NPAM-silica.

After the water and surfactant removed, the product turned to be white powder with a yield of 97%. Table 2 clearly showed the differences between the synthesis of hybrid silica and POSS. The used solvent was water for the synthesis of NPAM-silica, while great amount of organic solvent and hydrochloric acid were needed for the synthesis of POSS. It needed two steps to synthesize N-phenylaminomethyl POSS: hydrolytic condensation and then neutralization by Et_3N, while only one step for the synthesis of NPAM-silica. The yield of NPAM-silica was about 97% which was much higher than that of POSS (64%). From Table 2, it could be concluded that the route to synthesize NPAM-silica was economic and environmentally friendly.

Table 2. Comparisons between the synthesis of NPAM-silica and POSS.

Sample	Solvent	Steps	Yield
NPAM-silica	Water	One step	97%
POSS	Methanol, HCl, DMSO, Et_3N	Two steps: Hydrolytic condensation and neutralization	64%

There were five major peaks in solid stated ^{13}CNMR corresponding to the chemical shifts of -CH_2- (30 ppm) and phenyl ring (110 ppm-150 ppm) respectively. Solid stated ^{29}SiNMR showed a strong peak at about -70.9 ppm, meaning that the product was mainly T^3 structure. It also indicated the hydrolytic condensation of ND-42 in the emulsion process was sufficient. For other silanes, with the same synthetic route, such as vinyltriethoxysilane, usually formed T^2 and T^3 structures.[38]

Therefore, we could abbreviate the molecular formula of the product as $(PhNHCH_2SiO_{3/2})_n$. (Figure 2)

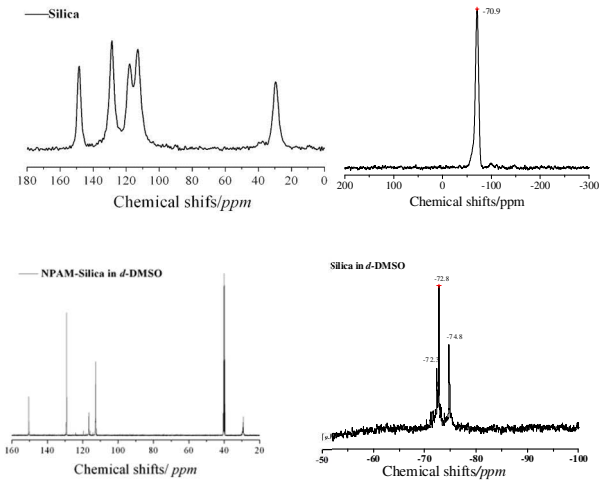

Figure 2. Solid state NMR and solution NMR of NPAM-silica. Solid state ^{13}CNMR (top left); Solid state ^{29}SiNMR (top right); Solution ^{13}CNMR (bottom left); Solution ^{29}SiNMR (bottom right).

XRD experiments were performed in order to further characterize the structure of NPAM-silica. As shown in Figure 3, there were two major peaks. One broad amorphous halo at about 20° was ascribed to the reason that different monomers known as T_8, T_{10}, T_{12}, T_9(OH), etc. (which could be found in Maldi-TOF MS) in NPAM-silica were haphazardly packed at the molecular level.[39, 40] The other sharp peak at about 5.5° corresponded to intramolecular distance between NPAM-silica[41, 42], which was in accordance with some other multifunctional polysilsesquioxanes.[39, 43, 44] This indicated that the molecules in the system were aggregated to form ordered structures to some extent.[41]

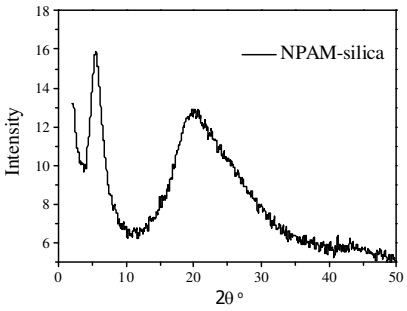

Figure 3. XRD of the NPAM-silica powder.

2. The solution of NPAM-silica

NPAM-silica was sphere-like with the size of 200 nm when the NPAM-silica emulsion was spin-coated on the silicon wafer. (Figure 4 left) Interestingly, the NPAM-silica could be dispersed in THF, acetone, DMF and DMAC readily and presented to be transparent dispersion. After the powder dispersing in organic solvents (1mg/L) and spin-coated on the

silicon wafer, the NPAM-silica turned to be nanoparticles with the size of 50 nm. (Figure 4 right) The dispersion was concentrated and NPAM-silica was then aggregated on the silicon wafer during the spin-coating process. The good solubility in organic solvents was ascribed to the multiple organic functional groups of NPAM-silica, which was similar with that of N-phenylaminomethyl POSS.[18, 41]

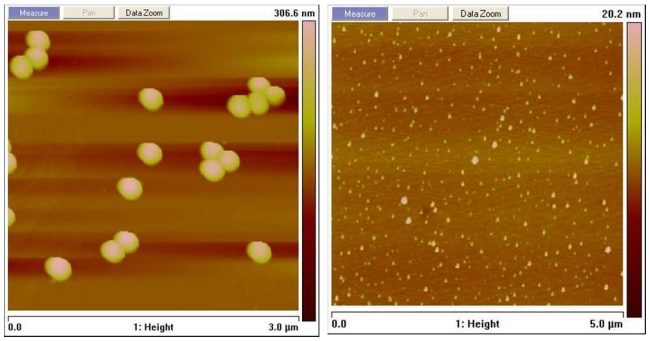

Figure 4. AFM of NPAM-silica samples spin-coated from emulsion (left) and spin-coated from DMAC dispersion (right).

The result of ^{13}CNMR in solution showed that the major chemical shifts of NPAM-silica did not change compared with those in solid state. Meanwhile, the result of ^{29}SiNMR in solution showed that the product in solution was mainly T^3 structure (Figure 2). According to the results of NMR in solution, it was concluded that the chemical structure of NPAM-silica did not change during the solution process.

The molecular weight of the NPAM-silica in THF was 1327 (M_w) characterized by GPC. The polydispersity (M_w/M_n = 1.08) remained low, and the result was consistent with other hydrolytic condensed silsesquioxane systems.[41]

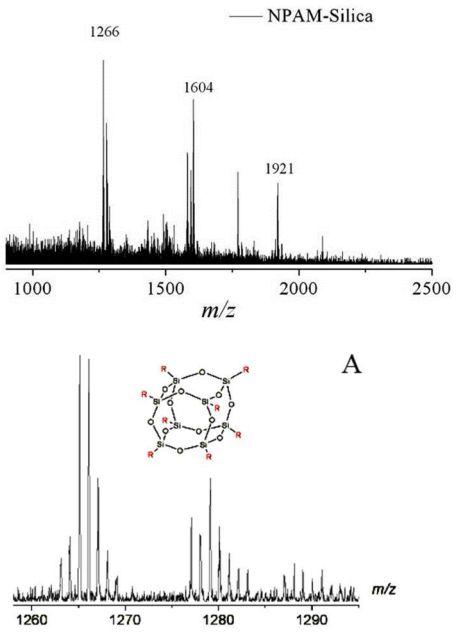

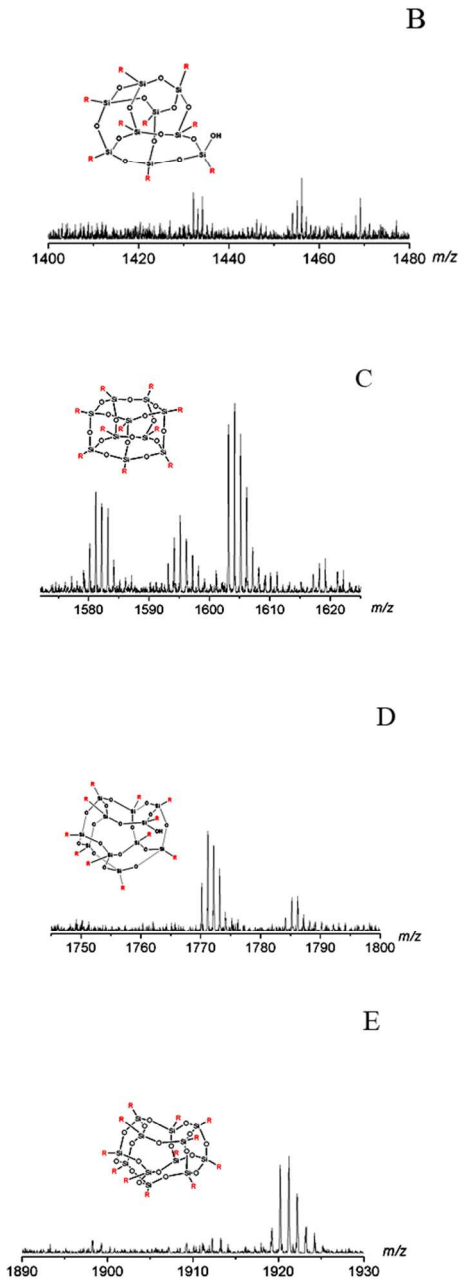

Figure 5. Maldi-TOF MS of NPAM-silica in the range of 1000-2500 m/z. (top) Maldi-TOF MS of NPAM-silica in the range of 1255-1295 m/z (A), 1400-1480 m/z (B), 1575-1625 m/z (C), 1745-1800 m/z (D) and 1890-1930 m/z (E). The corresponding structures were inserted in each figure from A to E, among them R meant the phenylaminomethyl group.

Maldi-TOF MS was used to analyze the molecular mass of the NPAM-silica. It showed that there were strong peaks at 1266, 1604 and 1921 which were corresponded to the fully condensed silsesquioxanes: $[T_8 + H]^+$, $[T_{10} + Na]^+$ and $[T_{12} + Na]^+$, respectively. However, there were also some peaks at 1458 [T_9

(OH) + Na] $^{+}$ and 1771 $[T_{11}(OH)+H]^{+}$ which were corresponded to the incompletely condensed silsesquioxanes. Figure 5 A to E showed the mass spectra of NPAM-silica in different molecular mass ranges. The possible structures were also inserted in the figures. It indicated that the product was the mixture of the fully condensed and a small quantity of incompletely condensed silsesquioxanes. Meanwhile, from the result of ^{29}SiNMR in solution (Figure 2 bottom right), the signal related to silanol structures did not appear. It was ascribed that the content of silanol groups in the product was below the detection limit.[26] The product was directly employed for further use, because the exclusion of time consuming process offered the possibility of large-scale production and practical application. Briefly, though there were different monomers in NPAM-silica, it could be more easily used in practice due to its facile synthesis than N-phenylaminomethyl POSS.

3. The reactivity of NPAM-silica with PU

Solid state ^{13}CNMR was performed to test the extent of reaction of the NPAM-silica when introduced into PU. The major change of chemical shifts was in the phenyl ring. For unreacted phenylaminomethyl groups, there were four main chemical shifts corresponding to four types of carbon atom in the phenyl ring. When the phenylaminomethyl group was reacted with isocyanate, the circumstance of the carbon atoms would change. The ortho-position (a) and para-position (b) corresponding to the 110-120 ppm in NPAM-silica (Figure 6. black line) would move to 130 ppm (a', b') in the NPAM-silica/PU composites (Figure 6. red line). The shift of carbon atom at meta-position would remain constant after reaction. Therefore, the degree of the reactivity could be checked by the residual peak at 110 ppm. From the figure, it was suggested that almost all of the NPAM-silica had been reacted with isocyanate when the loading reached 18 wt%, because nearly all peaks at 110-120 ppm were disappeared.

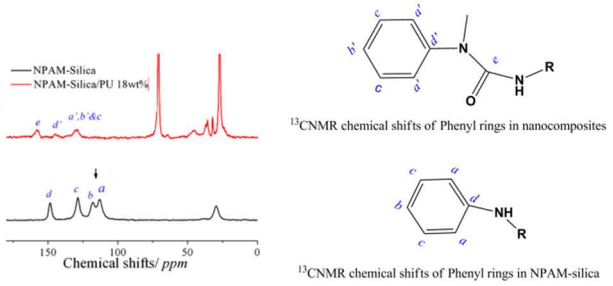

Figure 6. Solid state ^{13}CNMR of NPAM-silica and NPAM-silica/PU composites (left). Representative chemical structure of phenyl rings of NPAM-silica and the composites (right).

4. Morphology of NPAM-silica/PU composites

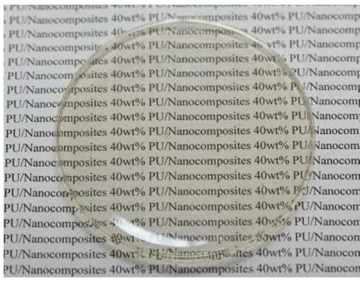

Figure 7. Typical picture of NPAM-silica/PU composite (PU40).

Figure 7 exhibited the typical picture of NPAM-silica/PU composite (PU40), which looked transparent. HRTEM was carried out to analyze the microstructure of NPAM-silica/PU composites. PU 18 was chosen to reveal the distribution of nanoparticles in the composites. Figure 8A showed alternately dark and bright features, which was attributed to the phase regions of hard and soft segments of POSS/PU nanocomposites. Interestingly, among these dark domains, it could be seen that considerable amounts of much darker spherical particles with the size of around 3 nm were uniformly dispersed in the NPAM-silica/PU networks. (Figure 8B) The dark nanoparticles could be attributed to NPAM-silica because of the high electron density of silicon atoms. It revealed that the silica was nano-dispersed in the hard phase region. The good compatibility could be attributed to the following two reasons: (1) there were physical interactions between multiple functional groups of NPAM-silica and PU.[45, 46] (2) almost all of the active groups of NPAM-silica were reacted with diisocyanate, and NPAM-silica was then introduced into the hard phase. This was consistent with the Solid state ^{13}CNMR result as mentioned above (Figure 6).

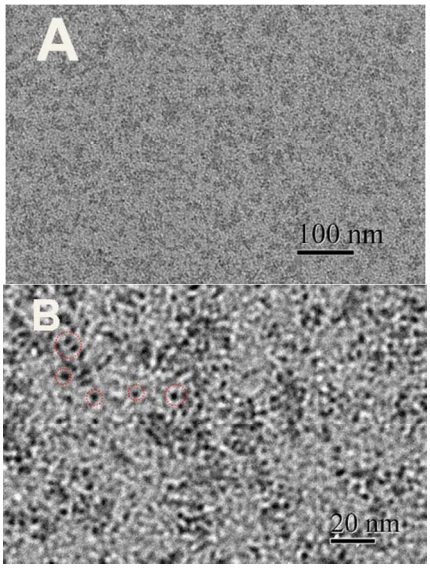

Figure 8. HRTEM figures of NPAM-silica/PU composite. (A). Scale bar 100 nm; (B). Scale bar 20 nm, much darker particles were labeled by red circles.

AFM also suggested the good compatibility of the NPAM-silica in PU. In Figure 9, PU18 presented a featureless surface in height image, and the roughness average (R_a) of the film was

0.229 nm which indicated the film was flat. PU18 showed alternately dark and bright features in phase contrast image. It revealed that the PU18 film had a two-phase heterogeneous structure with bright domains about 10 nm in diameter, which could be attributed to the microphase separation of the hard and soft segments in the PU. Meanwhile, a number of particles with much brighter contrast could be found in the phase images. It was reasonable to suggest that these particles were nano-dispersed NPAM-silica particles considering the AFM tip effect.

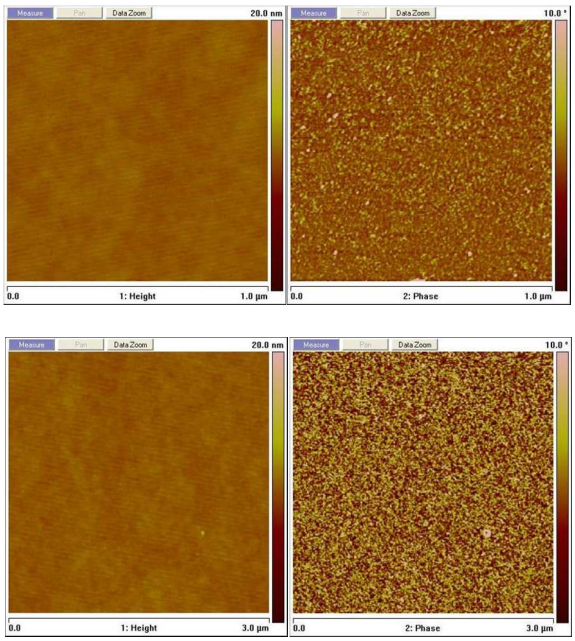

Figure 9. AFM (height image and phase image) of PU18 with different scales (1 µm and 3 µm).

5. The Mechanical properties of NPAM-silica/PU composites

5.1 DMA

DMA tests were performed to analyze the dynamic mechanical properties of the composites. The enhanced effect of the reactive NPAM-silica was obviously shown in Figure 10. When NPAM-silica concentration was less than 18wt%, the molar ratio of [NCO]/[NH] <1, the storage modulus of the composites increased with the increase of NPAM-silica concentration in almost all of the test temperature range. It was further described in two regions. (1) In the rubber plateau region, the length and the height of the rubber plateau of the composites increased regularly, which meant the cross-linking densities of the nanocomposites were increased as the concentration of NPAM-silica increased. Because the molecular weight between the cross-linking junctions decreased, the composites became more and more rigid. (2) In the wake of the rubber plateau region, the storage modulus of PU11 began to decrease at about 100 °C. When the NPAM-silica concentration reached 18 wt%, the rubber plateau could be preserved until 150 °C. This indicated that the addition of NPAM-silica could greatly enhance the service temperature of polyurethane.

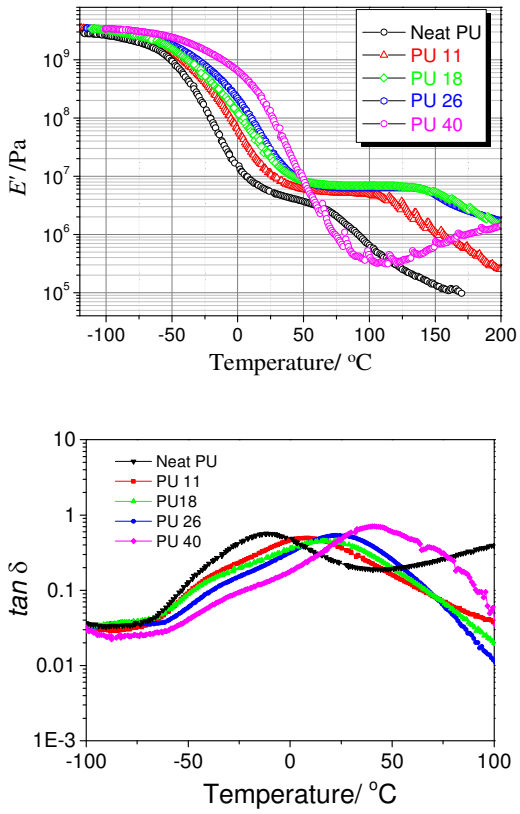

Figure 10. DMA of Neat PU and NPAM-silica/PU composites.

When the silica loadings reached 18 wt%, the amount of NPAM-silica was exactly satisfied with [NCO]/[NH] = 1. From ^{13}CNMR results of NPAM-silica nanocomposites, all the functional groups of NPAM-silica were reacted. On one hand, the modulus would increase by the addition of fillers. On the other hand, the increase of NPAM-silica amount would result in the decrease of the effective extent of reaction for per unit of NPAM-silica, thus led to the decrease of crosslinking densities. As a result, the storage modulus at rubber plateau region did not change too much with slightly excessive NPAM-silica (PU26) compared with PU18. It could be attributed to the combined effects of crosslinking density contribution and nanofiller addition contribution. When NPAM-silica concentration increased further, such as PU40, the molar ratio of [NCO]/[NH] exceeded 1 too much. The crosslinking density of the composites would decrease. Therefore, the storage modulus of PU40 at rubber plateau would decline compared with PU18.

Temperature dependence of tan δ was also plotted as shown in Figure 10. In order to obtain the value, loss moduli vs. temperature was also plotted (Figure S2, ESI), T_gs of both soft segments and hard segments were summarized in Table S1. On one hand, T_g of soft segments did not change much when the NPAM-silica loading was below 26wt%, while T_g of soft segments of PU40 increased about 10 K compared with other nanocomposites. On the other hand, T_g of hard segments increased gradually as NPAM-silica loadings increased. Because NPAM-silica reacted with the

diisocyanate, it is naturally to believe that NPAM-silica entered in hard segment phase. Interestingly, when the silica loading was excess too much ([NH]/[NCO]>1), some of the NPAM-silica would enter into the soft segment phase and hindered the motion of soft segment, which resulted in the increase of T_g of the soft segments of PU40. The amounts of the total hard segments (which were composed of IPDI, NPAM-silica, BD) were increased as NPAM-silica loadings increased, hence, T_g of hard segments increased.[47]

5.2 Tensile test at constant T_{test}-T_g

Tensile test was performed to investigate the enhanced mechanical properties of the composites. Considering the state of different samples, the test temperature of different samples was performed at constant T_{test}-T_g. (Here, T_g referred to that of the hard segment.) The constant T_{test}-T_g was chosen as 35K, because all the composites were in the rubber plateau under this situation. The stress-strain curves were expressed in Figure 11A. According to the typical rubber equation, the young's modulus at low strains follows:

$$E = \frac{3\rho RT}{Mc}\left(1-\frac{2Mc}{Mn}\right) \quad (1)$$

Where E stands for the Young's Modulus, M_c means the average molecular weight between the crosslinking junctions. The value of the young's modulus could be obtained from the slope of the tensile curve at initial part. We plotted young's modulus versus NPAM-silica loadings in Figure 11B. Obviously the young's modulus of the NPAM-silica/PU nanocomposites increased with the increase of NPAM-silica loadings. Based on the DMA result, the excess NPAM-silica did not further enhance the young's modulus of PU26 compared with that of PU18 in the temperature range of measurement.

Nevertheless, from the equation, we could find that the young's modulus was affected by the test temperature. Because samples were measured at different temperatures, the young's modulus would be different. In order to avoid the effect of temperature, *E/T* was also plotted versus NPAM-silica loadings. (Figure 11C) It showed almost the same trend as the young's modulus did. Therefore, under the same T_{test}-T_g conditions, the enhanced effect of the introduction of NPAM-silica was obvious without regard to T_g.

We also plotted storage modulus versus $T_g + T$ in order to check the results of tensile test at constant T_{test}-T_g. (Figure 11D) The modulus was enhanced with the increase of NPAM-silica loadings up to 18 wt%. When the content of NPAM-silica reached 26 wt%, the modulus of PU26 decreased a little, which showed the same trend as *E/T* did. Because the number of the active groups of NPAM-silica was excess, it would lead to the decrease of crosslinking densities.

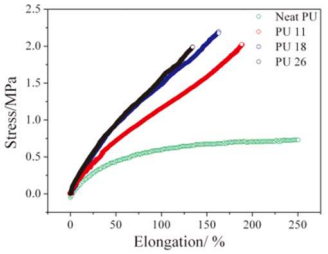

(A)

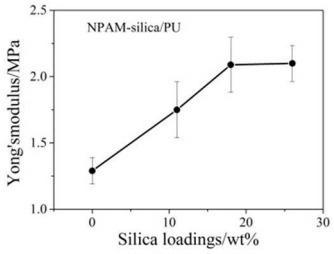

(B)

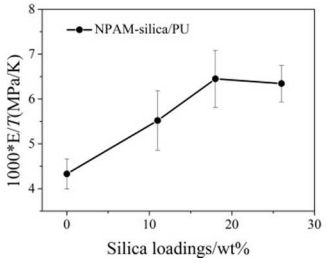

(C)

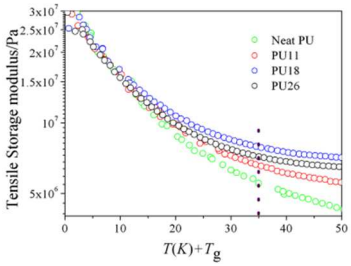

(D)

Figure 11. (A).Tensile tests at constant T_{test} - T_g; (B).Young's modulus (E) and versus NPAM-silica loadings; (C) Young's modulus/T_{test} (E/T) versus NPAM-silica loadings; (D) Storage modulus versus T_g+T according to DMA test.

5.3 Entropic effect and nanofiller effect

In polymer nanocomposites, the reinforcement in modulus often comes from two aspects. One is the modulus increase simply caused by the adding of fillers. The other is the entropic effect of the building network if the fillers act as a cross-linker in composites. However, it is seldom to investigate these two contributions separately.

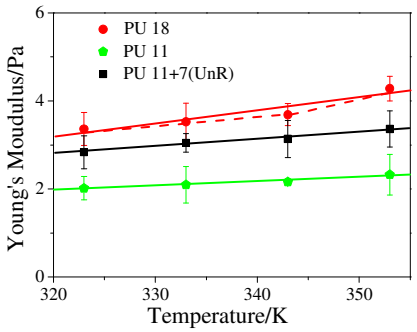

Figure 12. Temperature dependence of Young's modulus of NPAM-silica/PU composites at rubber plateau.

The entropic effect of the network is described by the well-known rubber equation, where the proportionality factor , (ρR/Mc) , between the modulus and temperature is corresponding to the crosslinking density (Equation 1). Temperature dependence of Young's modulus in the plateau region of varied composite systems was then performed to investigate the entropic effect in our nanocomposites. All the samples were tested at their rubber regions (323K, 333K, 343K and 353K). As shown in Figure 12, all the samples showed a slight increase in Young's modulus when temperature increased. The Young's modulus increased with temperature because of the increased thermal or Brownian motion, which caused the stretched molecular segments to tug at their "anchor points" and try to assume a more probable coiled-up shape.[48] Moreover, the cross-linking density of PU18 was higher than that of PU11 since it showed larger slope, indicating that the entropic effect was a contribution of the enhancement.

In order to separate the entropic contribution from the effect of addition of filler, we also tested the composite of PU11 + 7(UnR). The sample PU11 + 7(UnR) was composed of 11wt% NPAM-silica and 7wt% Phenyl-hybrid silica (a similar hybrid silica without reactive group), where the "UnR" part had similar chemical structure of NPAM-silica but couldn't act as cross-linker. Our observation showed that the trends of modulus change of PU11 and PU11 + 7(UnR) were almost the same which indicated the crosslinking densities of these two samples were nearly the same, but the Young's Modulus increased with the filler addition increased. So the nanofiller addition was the other contribution of the enhancement effect. This indicated that the reinforcement effect was derived from both entropic contribution and nanofiller contribution.

Besides, from the dash line of PU18, it could be found that the trend of modulus change was almost the same with PU11 and PU11 + 7(UnR) at low test temperatures, while at high test temperature, the trend increased. This suggested that the entropic contribution was obvious at high test temperature while nanofiller contribution was much obvious at low temperature.

6. Comparison NPAM-silica/PU composites with POSS/PU composites

In our previous work, we had introduced *N*-phenylaminomethyl POSS into PU network and obtained enhanced POSS/PU nanocomposites.[18] It was worth comparing the DMA results of NPAM-silica/PU nanocomposites with those of POSS/PU nanocomposites. (Figure 13) For the additive loadings of 11 wt% and 18 wt%, the storage moduli were almost the same in the glassy state. While in the rubber state, a great difference could be found. There was a rubber plateau for NPAM-silica/PU nanocomposites, but not for POSS/PU nanocomposites. The storage modulus of NPAM-silica/PU 18wt% at 100 °C was 6.9 MPa, which was 3 times larger than that of POSS/PU 18wt% (1.7 MPa). Besides, fewer loadings were needed for the NPAM-silica/PU composites to reach the rubber plateau than for the POSS/PU composites. This indicated the great advantage of NPAM-silica which would save the cost of raw material to achieve the same reinforced properties.

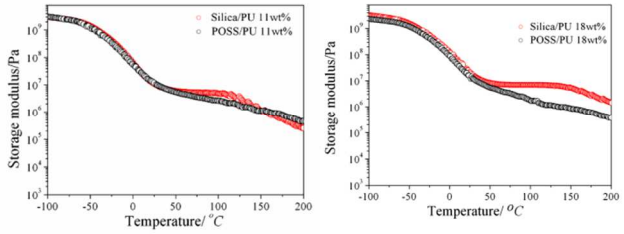

Figure 13. Comparison of dynamic mechanical properties between POSS/PU and NPAM-silica/PU composites (loadings are 11 wt% and 18 wt% respectively).

The results were intuitively confirmed by HRTEM. Figure 14 showed the high resolved pictures of the crosslinking junctions in two typical nanocomposites. In POSS/PU, POSS aggregated orderly to form a nano-crystal with the size of ca. 5-10 nm. While in NPAM-silica/PU, the NPAM-silica presented to be amorphous nanoparticles with the size about 3 nm and no lattice fringe was appeared. This revealed different crosslinking junctions in two nanocomposites. In POSS/PU composites, POSS tended to form nano-crystals in the PU network due to the interactions between POSS, and then orderly aggregated. The para-crystallization structure formation was previously reported in other POSS/polymer system.[27,49] The crystallization would hinder the inner functional groups to fully react with isocyanate. As to NPAM-silica, because it had smaller bulk and was not easy to form crystals, much more active groups would participate in the reaction. Therefore, when the loadings were high, the NPAM-silica could be well dispersed and incorporated in PU uniformly, while POSS tended to form the inhomogeneity network to some degree.

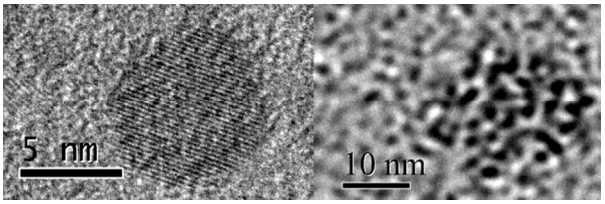

Figure 14. Comparison of POSS (left) and NPAM-silica particles (right) in POSS/PU and NPAM-silica/PU composites.

SAXS curves for POSS/PU and NPAM-silica/PU composites were displayed in Figure 15. It showed dependence of a logarithm of scattered X-ray intensity on the wave vector q. The curves revealed that there were microphase separations in the composites. The nano-sized domains were enriched with the inorganic phase (POSS or NPAM-silica). The peak position (q_{max}) was indicative of mean inter-domain spacing d, by $d=2\pi/q_{max}$. It could be seen that the scattering curve of NPAM-silica/PU was characterized with a well pronounced maximum corresponding to the wave vector 1.70 nm^{-1}, which was a signature of spatial periodicity of 3.7 nm. On the other hand, the peak of POSS/PU had much higher intensity and shifted towards a lower value of the wave vector 0.75 nm^{-1} corresponding to a periodicity of 8.3 nm. This indicated that POSS formed nanocrystal enriched domains in the composites which had much higher scattering density. The mean inter-domain spacing of POSS/PU composites was longer than that of NPAM-silica/PU composites.

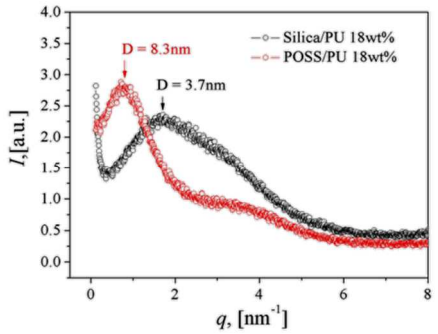

Figure 15. Desmeared small angle x-ray diffractograms of POSS/PU and NPAM-silica/PU nanocomposites.

Finally, three points were suggested to describe the differences of POSS/PU and NPAM-silica/PU nanocomposites. (1) The size of the crosslinking junctions of POSS/PU was larger than that of NPAM-silica/PU. For POSS/PU, it was about 5-10 nm, while about 3 nm for NPAM-silica/PU. The spatial distance of POSS or NPAM-silica enriched domains was different. For POSS/PU, it was 8.3 nm, while 3.7 nm for NPAM-silica/PU. (2) The states of the crosslinking junctions were different. POSS tended to form nanocrystal domains in the network, while the NPAM-silica was well dispersed in the network in the form of nanoparticles. (3) The effective numbers of reactive groups were different. Because of the formation of crystal in POSS, it would hinder the inner functional groups to participate in the reaction, and the effective amount of reactive groups in the reaction in POSS/PU was less than that in NPAM-silica/PU. These factors would result in the different crosslinking densities of the composites; hence the moduli at rubber plateau were different.

Conclusions

In summary, we provided an economic route to synthesize NPAM-silica. The NPAM-silica could be easily dispersed in organic solvents. The NPAM-silica in solution was mainly T^3 structure and the weight average molecular weight was 1327 with low polydispersity. Maildi-TOF MS and NMR results suggested that NPAM-silica was mainly composed of fully condensed silsesquioxanes and less partially condensed silsesquioxanes.

The NPAM-silica was then chemically incorporated into polyurethane, which acted as a chemical cross-linker. It showed excellent compatibility with PU and nano-dispersed in hard domains. The mechanical properties were greatly enhanced with the increase of NPAM-silica amount. The storage modulus and glass transition temperature were regularly increased with the increase of NPAM-silica amount when the loading of NPAM-silica was below 26 wt%. Young's modulus of the NPAM-silica/PU composites was also increased with the increase of the NPAM-silica amount without regard to the T_g. The enhancement in modulus came from both nanofiller addition and entropic contribution which was tested by temperature dependence of Young's modulus in rubber region. Compared POSS/PU with NPAM-silica/PU, it could be found that the storage modulus of the NPAM-silica/PU was higher than that of POSS/PU in rubber plateau. The size of crosslinking junctions in POSS/PU was larger than that in NPAM-silica /PU. The spatial distance between POSS enriched domains was also larger than that between NPAM-silica enriched domains. POSS formed crystals with the size of 5-10 nm in the composites while NPAM-silica formed nanoparticles with the size of 3 nm. This resulted in the higher degree of reactivity and higher crosslink densities for NPAM-silica/PU. Finally, the NPAM-silica provided a new alternative for polymer/nanocomposite in practical application which had the great advantages compared with POSS.

Acknowledgements

The authors would like to thank the Program for Changjiang Scholars and Innovative Research Team in University for financially supporting this research.

Notes and references

[a] *State Key Laboratory of Coordination Chemistry, Nanjing University*
[b] *Department of Polymer Science and Engineering, Nanjing University*
[c] *Nanjing National Laboratory of Microstructures, Nanjing University, Nanjing 210093, P.R. China. Fax: +86-25-836213371; Tel: +86-25-83593041; E-mail: jiaxd@nju.edu.cn; xikai@nju.edu.cn*
Electronic Supplementary Information (ESI) available

1. L. Schadler, *Nature Materials*, 2007, **6**, 257-258.
2. M. R. Bockstaller, R. A. Mickiewicz and E. L. Thomas, *Advanced Materials (Weinheim, Germany)*, 2005, **17**, 1331-1349.
3. V. Mittal, *Polymer Nanocomposites*, 2009, 143-152.
4. M. Qu, F. Deng, S. M. Kalkhoran, A. Gouldstone, A. Robisson and K. J. Van Vliet, *Soft Matter*, 2011, **7**, 1066-1077.

5. Y. Konishi and M. Cakmak, *Polymer*, 2005, **46**, 4811-4826.
6. W. Zhang, R. S. Blackburn and A. Dehghani-Sanij, *Scripta Mater*, 2007, **57**, 949-952.
7. D. W. Janes, J. F. Moll, S. E. Harton and C. J. Durning, *Macromolecules*, 2011, **44**, 4920-4927.
8. J. S. Meth, S. G. Zane, C. Z. Chi, J. D. Londono, B. A. Wood, P. Cotts, M. Keating, W. Guise and S. Weigand, *Macromolecules*, 2011, **44**, 8301-8313.
9. C.-J. Chen, M.-H. Tsai, I. H. Tseng, A.-W. Hsu, T.-C. Liu and S.-L. Huang, *RSC Advances*, 2013, **3**, 9729.
10. S. H. Stelzig, M. Klapper and K. Muellen, *Advanced Materials (Weinheim, Germany)*, 2008, **20**, 929-932.
11. N. Bitinis, M. Hernandez, R. Verdejo, J. M. Kenny and M. A. Lopez-Manchado, *Advanced Materials (Weinheim, Germany)*, 2011, **23**, 5229-5236.
12. V. Mittal, *Polymer Nanocomposites*, 2009, 1-14.
13. D. L. Green and J. Mewis, *Langmuir*, 2006, **22**, 9546-9553.
14. C. K. Wu, K. L. Hultman, S. O'Brien and J. T. Koberstein, *J Am Chem Soc*, 2008, **130**, 3516-3520.
15. K. Tanaka and Y. Chujo, *Journal of Materials Chemistry*, 2012, **22**, 1733-1746.
16. Y.-J. Lee, S.-W. Kuo, C.-F. Huang and F.-C. Chang, *Polymer*, 2006, **47**, 4378-4386.
17. Y. D. Zhang, S. H. Lee, M. Yoonessi, K. W. Liang and C. U. Pittman, *Polymer*, 2006, **47**, 2984-2996.
18. Q. H. Zhang, H. He, K. Xi, X. Huang, X. H. Yu and X. D. Jia, *Macromolecules*, 2011, **44**, 550-557.
19. W. Zhou, S. Yuan, L. Tan, Y. Chen and Y. Huang, *Polymer Engineering and Science*, 2012, **52**, 2063-2070.
20. H. Pan and Z. Qiu, *Macromolecules*, 2010, **43**, 1499-1506.
21. O. Monticelli, A. Fina, A. Ullah and P. Waghmare, *Macromolecules*, 2009, **42**, 6614-6623.
22. G. M. Kim, H. Qin, X. Fang, F. C. Sun and P. T. Mather, *Journal of Polymer Science Part B-Polymer Physics*, 2003, **41**, 3299-3313.
23. Y. Zhang, S. H. Lee, M. Yoonessi, H. Toghiani and C. U. Pittman, Jr., *Journal of Inorganic and Organometallic Polymers and Materials*, 2007, **17**, 159-171.
24. P. Chen, X. Huang, Q. Zhang, K. Xi and X. Jia, *Polymer*, 2013, **54**, 1091-1097.
25. H. Mori, A. H. E. Muller and J. E. Klee, *Journal of the American Chemical Society*, 2003, **125**, 3712-3713.
26. H. Mori, M. G. Lanzendorfer, A. H. E. Muller and J. E. Klee, *Macromolecules*, 2004, **37**, 5228-5238.
27. V. N. Bliznyuk, T. A. Tereshchenko, M. A. Gumenna, Y. P. Gomza, A. V. Shevchuk, N. S. Klimenko and V. V. Shevchenko, *Polymer*, 2008, **49**, 2298-2305.
28. T. Matsumoto, Y. Takayama, N. Wada, H. Onoda, K. Kojima, H. Yamada and H. Wakabayashi, *Journal of Materials Chemistry*, 2003, **13**, 1764-1770.
29. F. Dong, W. Guo, S.-S. Park and C.-S. Ha, *Journal of Materials Chemistry*, 2011, **21**, 10744-10749.
30. D. Lee, Y. A. Kim, Y. B. Kim, J. K. Kim and Y. K. Han, *Macromol Res*, 2008, **16**, 353-359.
31. Z. H. Zhou, J. M. Xue, H. S. O. Chan and J. Wang, *Mater Chem Phys*, 2002, **75**, 181-185.
32. W. Zhang, R. S. Blackburn and A. A. Dehghani-Sanij, *Scripta Mater*, 2007, **56**, 581-584.
33. C. Perruchot, M. M. Chehimi, M. Delamar, S. F. Lascelles and S. P. Armes, *J Colloid Interf Sci*, 1997, **193**, 190-199.
34. G. Y. Bae, J. Jang, Y. G. Jeong, W. S. Lyoo and B. G. Min, *J Colloid Interf Sci*, 2010, **344**, 584-587.
35. D. J. Liaw, C. C. Huang and B. Y. Liaw, *Polymer*, 1998, **39**, 3529-3535.
36. H. S. Xia and M. Song, *Soft Matter*, 2005, **1**, 386-394.
37. N. Dolmaire, F. Mechin, E. Espuche and J. P. Pascault, *Journal of Polymer Science Part B-Polymer Physics*, 2006, **44**, 48-61.
38. Z. Meng, C. Y. Xue, Q. H. Zhang, X. H. Yu, K. Xi and X. D. Jia, *Langmuir*, 2009, **25**, 7879-7883.
39. P. S. G. Krishnan and C. B. He, *Journal of Polymer Science Part a-Polymer Chemistry*, 2005, **43**, 2483-2494.
40. J. Zhang, R. W. Xu and D. S. Yu, *European Polymer Journal*, 2007, **43**, 743-752.
41. H. Mori, C. Sada, T. Konno and K. Yonetake, *Polymer*, 2011, **52**, 5452-5463.
42. R. M. Laine and M. F. Roll, *Macromolecules*, 2011, **44**, 1073-1109.
43. J. Zhang, R. Xu and D. Yu, *European Polymer Journal*, 2007, **43**, 743-752.
44. W. Li, F. Liu, L. Wei and T. Zhao, *Journal of Applied Polymer Science*, 2007, **104**, 3903-3908.
45. N. Hao, M. Boehning and A. Schoenhals, *Macromolecules*, 2007, **40**, 9672-9679.
46. N. Hao, M. Bohning, H. Goering and A. Schonhals, *Macromolecules*, 2007, **40**, 2955-2964.
47. A. K. Nanda, D. A. Wicks, S. A. Madbouly and J. U. Otaigbe, *Macromolecules*, 2006, **39**, 7037-7043.
48. D. W. Van Krevelen and K. Te Nijenhuis, *Properties of polymers: their correlation with chemical structure; their numerical estimation and prediction from additive group contributions*, Access Online via Elsevier, 2009.
49. B. Alvarado-Tenorio, A. Romo-Uribe and P. T. Mather, *Macromolecules*, 2011, **44**, 5682-5692.

N-phenylaminomethyl hybrid silica, a better alternative to achieve reinforced PU nanocomposites

Qiuhong Zhang, Xin Huang, Zhen Meng, Xudong Jia and Kai Xi**

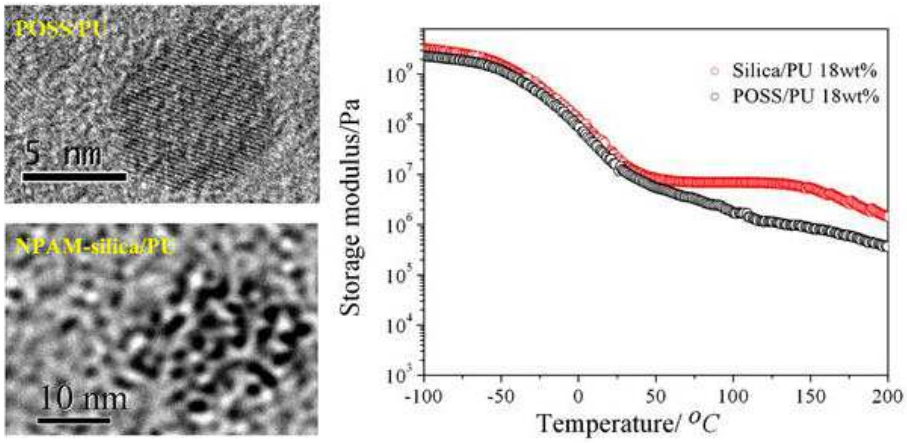

A novel NPAM-silica was synthesized with an economic and environmentally friendly method. It was chemically cooperated into polyurethane with enhanced mechanical properties. Compared with *N*-phenylaminomethyl POSS/PU composites, though the loadings and the functional groups were the same, the crosslinking junction states and the mechanical properties were different. NPAM-silica provided a new alternative for polymer/nanocomposite in practical application.